

Radio Properties of the Supernova Remnant N157B

J S Lazendic¹

*Centre for Astronomy, University of Western Sydney, PO Box 10, Kingswood NSW 2747, Australia
Australia Telescope National Facility, CSIRO, PO Box 76, Epping NSW 1710, Australia*

J R Dickel

*Astronomy Department, University of Illinois at Urbana-Champaign, 1002 West Green Street, Urbana IL
61801, USA*

R F Haynes

*Australia Telescope National Facility, CSIRO, PO Box 76, Epping NSW 1710, Australia
and*

P A Jones and G L White

Centre for Astronomy, University of Western Sydney, PO Box 10, Kingswood NSW 2747, Australia

ABSTRACT

A new investigation of the supernova remnant (SNR) N157B was carried out with the Australia Telescope Compact Array. Radio continuum images of the entire 30 Doradus region have been made at 3.5 and 6 cm wavelength with a resolution of $\sim 2''$. These data allow a high resolution study of the spectral index distribution and polarization properties of both N157B and the nearby 30 Doradus nebula (the latter will be reported in a subsequent paper). N157B is an extended Crab-type SNR which may be beginning the transition to a composite remnant. There is little apparent fine structure and the brightest radio region is several parsecs from the probable position of the X-ray pulsar. The SNR has a radio spectral index of -0.19 and is significantly polarized at 3.5 cm but not at longer wavelengths.

Subject headings: radio continuum: interstellar — supernova remnants: individual (N157B) — galaxies: individual (LMC)

1. Introduction

N157B (Henize 1956) (also 30 Dor B or SNR 0538–691) is a supernova remnant located near the edge of the 30 Doradus nebula (Bode 1801) in the Large Magellanic Cloud (LMC). The 30 Doradus complex is the nearest extragalactic giant H II region and an active star-forming region (Chu et al. 1992). The nebula and the SNR are in the same interstellar region of the LMC as SN1987A

and other SNRs, among which is SNR 0540–693, a composite remnant with a pulsar and a plerion component (Manchester et al. 1993). The SNR nature of N157B was first determined by its excess of radio over optical emission (Le Marne 1968), and confirmed by the detection of [S II] lines in the optical spectrum (Danzinger et al. 1981).

The Crab nebula represents the class of plerionic supernova remnants; it contains a pulsar as a central energy source and a well-organised magnetic field indicated by strong linear polarization at radio wavelengths and relatively flat radio spectrum

¹Current address: Astrophysics Department, School of Physics A29, University of Sydney, NSW 2006, Australia

(Weiler 1983). A number of detected SNRs have radio characteristics similar to the Crab nebula, yet the pulsar stimulation of the synchrotron nebula is confirmed for just a few of them (Seward 1983, 1989; Weiler 1988). N157B is classified as a Crab-type remnant because of its centre-filled morphology, flat radio spectrum (Mills et al. 1978; Milne et al. 1980), and strong soft X-ray emission (Long & Helfand 1979).

Recently a 16 ms pulsar detected only in X-rays (Marshall et al. 1998; Gotthelf & Wang 1996; Wang & Gotthelf 1998) has been associated with N157B. Previous observations of N157B at radio wavelength have not detected any polarized emission (Dickel et al. 1994). However, our current investigation at a shorter wavelength shows a significant level of polarization. All of the data together confirm the classification of N157B as a Crab-type SNR.

The presence of N157B in a relatively dense and complex interstellar environment together with the younger SN1987A and the presumably older SNR 0540–693, offers a unique opportunity to study the evolution of Crab-type SNRs in such areas. The best Galactic examples, the Crab and 3C58, both appear to be in exceptionally low-density environments (Fesen 1997).

2. Observations and data reduction

2.1. General procedures

The first observations at 6 cm were carried out with the Australia Telescope Compact Array² (ATCA) in the period January – July 1993. Additional observations at 3.5 and 6 cm were obtained during May 1998 – June 1999. The six antennas were used in several different array configurations giving baselines with the range from 31 m to 6 km to provide good sampling of the observed region. Details of the ATCA can be found in Frater et al. (1992). The relevant observing parameters are given in Table 1.

The primary calibrator used in all observations was PKS B1934–638 with assumed flux densities of ~ 6 and 2.78 Jy at 6 and 3.5 cm respectively. PKS B0454–810 was used as secondary calibration

source.

The observations in 1998 – 1999 were done in mosaic mode with 20 pointing centres to cover the whole 30 Doradus region. The observing pattern was such that the pointing nearest to the SNR (field no. 15 – see Table 1) was observed after every five fields to improve signal-to-noise on this object. The data were taken simultaneously in 32×4 -MHz frequency channels of which the 26 central channels are used in the imaging procedure. They have been averaged down to 13×8 -MHz channels by Hanning smoothing and then to a single channel during imaging. The data were gridded and deconvolved according to the procedure for mosaic data sets (Sault & Killeen 1997). Separate images of field no. 15 alone were also produced.

The 3.5-cm images of the SNR were made by combining 7 fields (including no. 15) which had the pointing centre closest to the SNR. The deconvolution of all 7 fields was done together, which improves the deconvolution process but introduces some errors in the model of the primary beam. The edges of the mosaiced region have low sensitivity so the noise level across the mosaic image will vary. In the imaging process the primary beam attenuation will not be completely corrected, because that correction is constrained by the noise in the individual pointings, which can differ (Sault & Killeen 1997). In this case, the procedure limits the dynamic range of the final image to 100:1. We also made an image of field no. 15 alone. This was cleaned and corrected for the pattern of the primary beam. The peak brightness in both images is very close (~ 7 mJy/beam), but the single field image has lower signal-to-noise ratio over the entire field.

The image at 6 cm was constructed by combining four data sets at 4.8 GHz and pointing no. 15 from 4.4 GHz data (see Table 1). Thus, in addition to the mosaicing procedure explained above, the multi-frequency synthesis technique (Sault & Killeen 1997) was also used to produce the final image of the region. As in the previous case, an image of field no. 15 alone was made as well.

2.2. Polarization

The interferometer produces an instrumental polarization which increases outward from the cen-

²The Australia Telescope is funded by the Commonwealth of Australia for operation as a National Facility managed by CSIRO

TABLE 1
OBSERVATIONAL PARAMETERS.

Parameter	4.4 GHz	4.8 GHz	8.6 GHz
Date	1998 Aug 27 1998 Sep 26, Oct 2 1999 Jun 24	1993 Jan 16, 19, 29 1993 Jul 23	1998 May 1, 31, Aug 27 1998 Sep 26, Oct 22 1999 Jun 24
Configurations	6C, A, 1.5D, 375	750B, C, A, D	750A, E, 6C, A, 1.5D, 375
Field Center (J2000)	05 ^h 37 ^m 50 ^{sa} −69°10′00″ ^a	05 ^h 38 ^m 45 ^s −69°06′00″	05 ^h 37 ^m 50 ^{sa} −69°10′00″ ^a
Total bandwidth (MHz)	128	128	128
No. of frequency channels ..	32	32	32
FWHM of primary beam ...	10′	10′	5′

^afield no. 15 of a larger mosaic

ter of the primary beam pattern of the individual telescopes. In fields with the pointing centre away from the SNR for which an unpolarized source (30 Doradus) is at the half-power point, we found fractional polarizations up to $\sim 10\%$ with electric field vectors radially oriented with respect to the direction of the beam centre. This value of fractional polarization in the surrounding fields confirms that off-centre instrumental polarization is indeed strong.

Therefore, for the polarimetry we used only field no. 15 for which N157B is in the center of the beam and the instrumental polarization is low (0.3%). The images of the Q and U Stokes parameters were made in a similar way as the I image and combined to produce the image of polarized intensity. To create such an image we used the MIRIAD task IMPOL which statistically corrects the polarized intensity for Ricean bias (Sault & Killeen 1997). Noise in both the Q and U polarization images was below the $5\text{-}\sigma$ noise level of the total intensity image and CLEANing was not necessary.

The polarized intensity images of the SNR at 6 cm were made using only field no. 15 with the same procedure as for the single-field image explained above. The 1993 positions were not directly toward N157B and so were not included in the polarization analysis because of the off-axis effects discussed above. The fractional polariza-

tion in the direction of N157B was found to be $\sim 3\%$, near the instrumental value, thus confirming only that N157B is not highly polarized at this wavelength.

3. Results

3.1. 3.5 cm image

The high resolution total intensity image at 3.5 cm of the region around N157B was made using all six available configurations; it has a Gaussian beam of HPBW $\sim 2''$ (see Fig.1). It shows reasonably uniform brightness distribution and the center-filled morphology characteristic of Crab-type SNRs. We note that the bright peak is resolved. It lies about $12''$ (4 pc at the 50 kpc distance to the LMC) to the northwest of the X-ray peak, which is presumably the location of the pulsar (Wang & Gotthelf 1998). Also, the radio peak is not centered on the full SNR which extends well to the south with dimensions of about $120'' \times 70''$ or $30 \text{ pc} \times 18 \text{ pc}$. Slices along the major axis of the remnant at a position angle of about 150° show continuous emission throughout the total extent with a slight decrease near a declination of $-69^\circ 10' 50''$ and then a rise again to the south. Perhaps part of an outer shell may be forming around the plerion. The size given includes this outer emission.

This is the most sensitive high-resolution radio

image of this object now available, yet no direct evidence of the pulsar can be seen. This is not surprising, however, as 3.5 cm is a very short wavelength for pulsar emission which usually peaks at meter wavelengths. The pulsar has not been found at any radio wavelength.

We found strong linear polarization in the direction towards the SNR. The electric field vectors are superimposed on continuum contours in Fig.2. The mean fractional polarization is $\sim 10\%$, calculated by dividing the polarized intensity image of the source by the total intensity image (both made with field no.15 only). The total intensity values were truncated at the $3\text{-}\sigma$ level which is $\sim 5 \text{ mJy beam}^{-1}$ before division, but all (bias corrected) polarized intensities within the source boundaries given by the total intensity cutoff were used. In the vector display, the vectors were truncated at the $3\text{-}\sigma$ level. We note that a polarization map using seven mosaic positions looked similar but was noisier because of the few percent radial instrumental polarization toward N157B from the surrounding fields.

The electric vector alignment is fairly uniform but the polarized intensity is surprisingly patchy. The highest fractional polarization is 15.4% towards $05^{\text{h}}37^{\text{m}}44^{\text{s}}.5$ and $-69^{\circ}10'07''.5^3$, whereas at the position of the brightest total intensity $05^{\text{h}}37^{\text{m}}41^{\text{s}}.5$ and $-69^{\circ}09'31''.0$ it is 5%, which is the lowest fractional polarization (excluding blanked regions). At the position of the X-ray peak at $05^{\text{h}}37^{\text{m}}47^{\text{s}}.5$ and $-69^{\circ}10'17''.5$ the polarized intensity is 7%.

3.2. 6 cm image

The total intensity image of N157B at 6 cm (shown in Fig.3) was made using eight available configurations of the Compact Array (see Table 1) and also has the synthesized beam of HPBW $\sim 2''$. The fractional polarization towards N157B (calculated using only field no. 15) is only $\sim 3\%$, which is close to the noise level. We therefore detect no reliable polarization at 6 cm and conclude that there must be strong Faraday depolarization between 3.5 and 6 cm. We note that at 6 cm the distribution of the closest antenna spacings represents lower spatial frequencies than those seen at 3.5 cm. If the polarization is all on a fine spatial

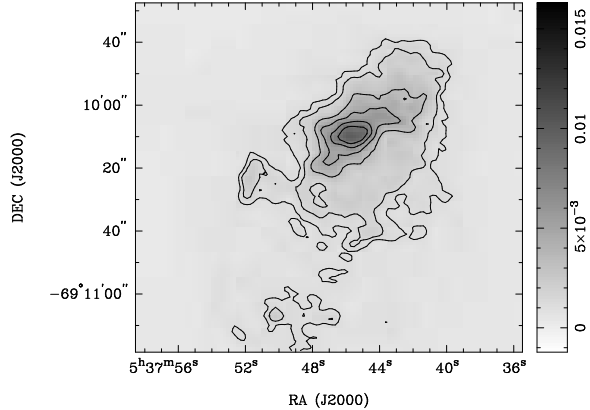


Fig. 1.— Radio continuum grayscale and contour image of N157B at 3.5 cm with HPBW of $2''.67 \times 1''.80$. The contour levels are: 1.1, 1.6, 3.3, 4.9, 6.5, 8.2 and $9.8 \text{ mJy beam}^{-1}$.

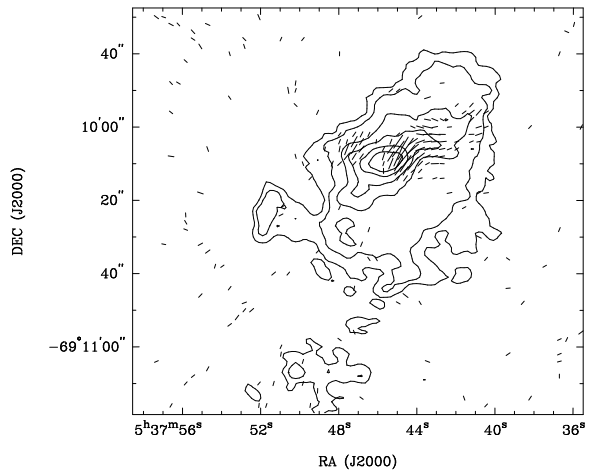


Fig. 2.— Image of the total intensity of N157B at 3.5 cm with \mathbf{E} -vectors superimposed. A vector length of $1''$ represents a linearly polarized intensity of $1.7 \text{ mJy beam}^{-1}$. The contour levels are: 1.1, 1.6, 3.3, 4.9, 6.5, 8.2 and $9.8 \text{ mJy beam}^{-1}$.

³all position are in J2000

scale we may find a lower value of the polarization at 6 cm. Inspection of Fig.2, however, shows that while there is fine structure a significant part of the 3.5-cm polarization is uniform on scales of over 10'' and so should appear at 6 cm. Depolarization effects are obviously present.

4. Discussion

N157B is very close to 30 Doradus and it is also embedded in an H II region around the OB association LH99 (Lucke & Hodge 1970). Chu et al. (1992) concluded that the southern part of the SNR is obscured and possibly interacts with the dark cloud within the H II region. With our high radio sensitivity we can see that the SNR does extend well to the south of the bright northern component. With a size of 30 pc \times 18 pc, it is the largest Crab-type SNR known. The feature at 05^h37^m52^s and -69°10'22'' and the elongated structure centered at about 05^h37^m50^s and -69°11'10'' might indicate the beginning of a transition into a composite remnant like SNR 0540-693. The dense interstellar environment of the 30 Doradus region may be conducive to the formation of a shell and the irregular structure of N157B may be accounted for by a complex density distribution.

Chu et al. (1992) found that N157B contributes up to 80% of the flux density in this region at 0.843 GHz, the rest coming from the surrounding H II region. They suggested that the flat radio spectral index (α) of -0.1 ($S_\nu \approx \nu^\alpha$) indicated from earlier measurements (Milne et al. 1980) should be characteristic of the SNR itself. However, they also found that the optical emission lines from N157B originate in conditions associated with blast waves and they therefore concluded that the corresponding non-thermal radio emission should not have the flat spectrum typically associated with pulsar stimulation. Our results below differ somewhat from the previously published values derived from low resolution data but still show that N157B has a flat radio spectrum.

Data used for determining the radio spectrum of N157B are listed in Table 2. To obtain a consistent background and source extent, the images were all convolved to the 43'' \times 45'' resolution of the MOST image and the integrated flux density calculated over the same area in each convolved map. A background intensity around the source

was determined from the average of several areas around the SNR but far enough from 30 Doradus to avoid contamination.

The resultant integrated flux densities listed in Table 2 give a mean spectral index for N157B of -0.19 (see Fig.4). Brightness-brightness plots also show that the spectrum does not vary significantly across the whole extent of the SNR. This argues that the entire SNR is pulsar-powered.

In the X-ray band, however, the spectrum of N157B differs slightly relative to other such remnants. It has a power-law energy slope of -1.5 which is steeper than those of other Crab-like remnants with values of about -1.0 (Wang & Gotthelf 1998). The X-ray and entire spectrum of N157B also strikingly resemble that of SNR 0540-693, leaving no doubt of the plerionic origin of N157B. The SNR 0540-693 contains a pulsar and is a composite remnant, sharing the characteristics of pure shell remnants and pure plerions (Seward 1989; Manchester et al. 1993). This latter composite SNR is often called a Crab-type remnant, because the core is Crab-like and the faint shell component was only investigated later. This further similarity between N157B and 0540-693 is more evidence that N157B is beginning the transition to a composite remnant.

The polarization properties of the 30 Doradus region were previously investigated by Dickel et al. (1994) at longer wavelengths. They used ATCA observations at 13 cm but concluded that no polarized emission was detected in any region of N157B above the level of instrumental polarization (less than 2%). We report a significant level of polarized emission at 3.5 cm from N157B for the first time. This relatively high level of 10% is typical for a Crab-type remnant. The data at 6 cm give a marginal detection which we consider an upper limit of 3% fractional polarization at the peak of N157B. This low level of polarized emission at this wavelength implies very strong internal depolarization. The observed polarization could also be reduced by the thermal emission from the associated H II region around LH99 which may be intertwined with the SNR so that its thermal electrons may cause some of the Faraday depolarization as well.

To estimate the internal rotation necessary to cause the observed depolarization, we use a slightly modified version of the relation given by

TABLE 2
FLUX DENSITIES OF N157B.

Frequency (GHz)	Flux Density (Jy)	References
0.843	2.86 ± 0.24	Anne Green (1997, private communication)
1.400	2.64 ± 0.16	Data of Mebold et al. (1997)
2.378	2.36 ± 0.14	Data of Dickel et al. (1994)
4.740	2.20 ± 0.10	Data of this paper
8.600	1.82 ± 0.12	Data of this paper

Burn (1966):

$$P(\lambda_2)/P(\lambda_1) = \sin(\delta)/\delta \quad (1)$$

where P is the fractional polarization at λ_2 , the longer wavelength, and λ_1 , the shorter wavelength; δ is the rotation in position angle of the measured electric vector between the two wavelengths. We will adopt the possible detection of 3% polarization at 6 cm and so use a rough mean value for $P(\lambda_2)/P(\lambda_1)$ of 0.3 which requires an average rotation of 135° . Then using the standard formula for Faraday rotation we can estimate the line-of-sight magnetic field strength:

$$\delta = 7.9 \times 10^5 \lambda^2 \int N_e \vec{B} \times d\vec{l} \quad (2)$$

where δ is in radians, λ is in meters, N_e is the electron density in cm^{-3} , B is the magnetic field strength in Gauss, and l is the path length through the SNR in pc. Because the Faraday rotation increases progressively along the path, we must actually find the adopted rotation along half the depth along the line of sight. We do not, of course, know this depth directly but choose its value to be approximately equal to the short observed axis of the SNR or a half depth of 10 pc. From an analysis of ROSAT and ASCA X-ray spectra, Wang & Gotthelf (1998) derived an electron density of $0.6f^{-0.5} \text{cm}^{-3}$, where f is the filling factor of the object. Because Crab-type SNRs should be reasonably uniform inside, we adopt a value for f of about 0.5 to get a mean density of about 2cm^{-3} . These numbers give a line-of-sight magnetic field strength of $30 \mu\text{Gauss}$. Most Crab-type SNRs have rather uniform magnetic fields; over the limited region where it can be observed, N157B shows

more variation than most. It may be that the field is directed mainly toward us, which would reduce the observed polarization at all wavelengths and also give a large Faraday rotation. No correction has been made for an unknown field orientation which would tend to increase the field strength in the remnant. We should emphasize that this result is only an order of magnitude estimate. Neglected factors include the uncertainties and probably variations in the depolarization, magnetic field reversals, density uncertainties and variations. For example, significant clumping can change the apparent integrated electron density because the X-ray emission depends upon the density squared but the Faraday rotation depends linearly on the density and the sum of squares does not equal the square of sums.

If we know the magnetic field strength, we can then determine the energy in relativistic electrons from the intensity of the synchrotron radiation. Ginzburg & Syrovatskii (1965) give the approximate formula:

$$E_e = \Sigma_\nu \times R^2 \times A \times \text{area} \times \text{pathlength} \times B^{-3/2} \quad (3)$$

where E_e is the total energy in relativistic electrons, Σ_ν is the surface brightness of the remnant at a given observing frequency ν , R is its distance, and A is a parameter that depends on the frequency, the spectral index and the adopted cutoff frequencies for the synchrotron radiation. There appears to be a break in the spectrum of the non-thermal emission between the radio and X-ray (Wang & Gotthelf 1998) but we do not know specifically where it occurs. We shall choose an upper frequency of 10^{12}Hz and a lower

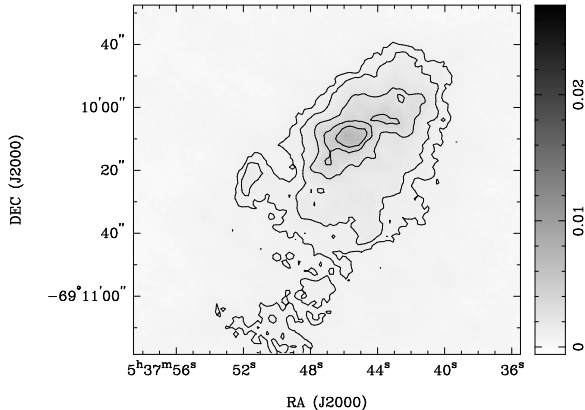


Fig. 3.— Radio continuum grayscale and contour image of N157B at 6 cm with HPBW of $1''.79 \times 1''.74$. The contour levels are: 0.9, 1.3, 2.4, 4.0, 5.4, 8.1, 10.8 and $13.5 \text{ mJy beam}^{-1}$.

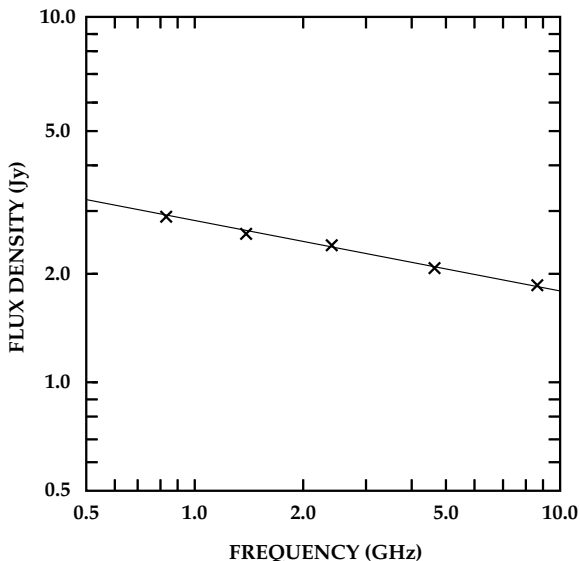


Fig. 4.— Radio spectrum of N157B. The slope of the fitted line is -0.19 .

one of 10^7 Hz , with a spectral index of -0.19 , $A = 3.7 \times 10^{19}$ at 8.6 GHz where the flux density is 1.82 Jy . With the sizes and magnetic field strength given above, we find that the mean relativistic electron energy density is $4 \times 10^{-10} \text{ ergs cm}^{-3}$. This is about 10 times the magnetic energy density. While within the errors, we cannot definitely state that the values are different. It is interesting to note that in the three objects for which we have now measured the relative energies by this method, each has between 3 and 10 times greater relativistic electron energy than magnetic energy (Kepler’s SNR Matsui et al. (1984) and N23 SNR Dickel & Milne (1998)).

Wang & Gotthelf (1998) give an approximate temperature for the thermal gas in N157B of $0.4 - 0.7 \text{ keV}$. Choosing 0.6 keV and the approximate density of 2 cm^{-3} used above, the thermal energy density is about $3 \times 10^{-9} \text{ erg cm}^{-3}$. Thus the thermal energy is about 10 times that in relativistic electrons and 100 times that in the magnetic field. Even in this Crab-type SNR the thermal energy dominates.

In summary, the filled structure and uniform spectral index of N157B are Crab-like but it also has some characteristics similar to those of the composite SNR 0540–693. Although the dense, irregular surroundings may be partly responsible for the non-uniform brightness and outline of this SNR particularly to the south, the overall morphology and spectral index suggest that this SNR is just beginning the transition from a pure Crab-like remnant to a composite remnant. It will be interesting to see how it changes at radio, optical and X-ray wavelengths in the future.

We have detected for the first time a significant level of linearly polarized emission in this object at 3.5 cm wavelength. The encompassing H II region and clumpy internal structure within the SNR may cause sufficient Faraday rotation to reduce the polarization to below detectable levels at 6 cm and make the large variations in the polarization observed at 3.5 cm at different positions around the remnant. Observations at higher frequencies, e.g. 23 GHz, are needed to enable more accurate determination of the Faraday rotation.

We thank M. Costa, D. Milne and H. Dickel for participating in the observing. We thank L. Staveley-Smith for the ATCA image at 21 cm and

helpful comments. We thank B. Gaensler and A. Green for providing us with the MOST image. JRD acknowledges support from the Campus Honours Program of the University of Illinois at Urbana-Champaign. JSL acknowledges support from the Astronomy DRG and the UWS Nepean Research Office. Work at UWS Nepean was also supported by the ARC. JSL thanks the ATNF for the use of their facilities, J. Whiteoak for useful comments on polarization, N. Killeen and R. Sault for valuable discussions on data reduction, and M. Filipovic.

REFERENCES

- Bode, J., 1801, ‘Allgemeine Beschreibung und Nachweisung der Gestirne’, Berlin: Beym Verfasser
- Burn, B. J., 1966, MNRAS, 133, 67
- Chu, Y.-H., Kennicutt Jr., R. C., Schommer, R. A. & Laff, J., 1992, AJ, 103, 1545
- Clarke, J. N., Little, A. G. & Mills, B. Y., 1976, Aust. J. Phys. Astrophys. Suppl., 40, 1
- Danziger, I. J., Goss, W. M., Murdin, P., Clark, D. H. & Boksenberg, A., 1981, MNRAS, 195, 33
- Dickel, J. R., Milne, D. K., Kennicutt, R. C., Chu, Y.-H. & Schommer, R. A., 1994, AJ, 107, 1067
- Dickel, J. R., Milne, D. K., 1998, AJ, 115, 1057
- Fesen, R. A. 1997, presented in ‘ 10^{51} Ergs,’ SNR Workshop, Minneapolis MN, 1997
- Frater, R. H., Brooks, J. W. & Whiteoak, J. B., 1992, J. of Electrical & Electronic Eng. Austr., 12, 103
- Ginzburg, V. L. & Syrovatskii, S. I., 1965, ARA&A, 3, 297
- Gotthelf, E. V. & Wang, Q. D., 1996, ‘Roentgenstrahlung from the Universe,’ MPE Report 263, 255
- Green, A., 1997, private communication
- Green, D. A., 1996, ‘A catalogue of galactic supernova remnants’, Cambridge: Mullard Radio Astronomy Observatory, 1996 August version
- Haynes, R. F., Klein, U., Wayte, S. R., Wielebinski, R., Murray, J. D., Bajaja, E., Meinert, D., Buczillowski, U. R., Harnett, J. I., Hunt, A. J., Wark, R. & Sciacca, L., 1991, A&A, 252, 475
- Henize, K. G., 1956, ApJS, 2, 315
- Le Marne, A. E., 1960, MNRAS, 139, 461
- Long, K. S. & Helfand, D. J., 1979, ApJ, 234, L77
- Lucke, P. B. & Hodge, P. W., 1970, AJ, 75, 171
- Manchester, R. N., Staveley-Smith, L. & Kesteven, M. J., 1993, ApJ, 411, 756
- Marshall, F. E., Gotthelf, E. V., Zhang, W., Middleditch, J. & Wang, Q.D., 1998, ApJ, 499, L179
- Matsui, Y., Long, K. S., Dickel, J. R. & Greisen, E. W., 1984, ApJ, 287, 295
- Mebold, U., Deusterberg, C., Dickey, J. M., Staveley-Smith, L. & Kalberla, P., 1997, ApJ, 490, 65
- Milne, D. K., Caswell, J. L. & Haynes, R. F., 1980, MNRAS, 191, 496
- Mills, B. Y., Turtle, A. J. & Watkinson, A., 1978 MNRAS, 185, 263
- Sault, R. J. & Killeen, N., 1997, ‘Miriad Users Guide,’ ATNF Publication
- Seward, F. D., 1983, in ‘Supernova Remnants and their X-Ray Emission’, IAU Symp. 101, (eds.) J. Danziger & P. Gorenstain, (Dordrecht, Kluwer), 405
- Seward, F. D., 1989, Space Science Reviews, 49, 385
- Wang, Q. D. & Gotthelf, E. V., 1998, ApJ, 494, 623
- Weiler, K. W., 1983, in ‘Supernova Remnants and their X-Ray Emission’, IAU Symp. 101, (eds.) J. Danziger & P. Gorenstain, (Dordrecht, Kluwer), p. 299
- Weiler, K. W. & Sramek, R. A., 1988, ARA&A, 26, 295